Role of Active Site Histidines in the Two Half-Reactions of the Aryl-Alcohol Oxidase Catalytic Cycle

Aitor Hernández-Ortega,[#,†] Fátima Lucas,[#,‡] Patricia Ferreira,[§] Milagros Medina,[§] Victor Guallar,*[,‡,||] and Angel T. Martínez*[,†]

[†]Centro de Investigaciones Biológicas, CSIC, Ramiro de Maeztu 9, E-28040 Madrid, Spain

[‡]Joint BSC-IRB Research Program in Computational Biology, Barcelona Supercomputing Center, Jordi Girona 29, E-08034 Barcelona, Spain

[||]Institució Catalana de Recerca i Estudis Avançats (ICREA), Passeig Lluís Companys 23, E-08010 Barcelona, Spain

[§]Department of Biochemistry and Molecular and Cellular Biology and Institute of Biocomputation and Physics of Complex Systems, University of Zaragoza, E-50009 Zaragoza, Spain

S *Supporting Information*

ABSTRACT: The crystal structure of aryl-alcohol oxidase (AAO), a flavoenzyme involved in lignin degradation, reveals two active-site histidines, whose role in the two enzyme half-reactions was investigated. The redox state of flavin during turnover of the variants obtained show a stronger histidine involvement in the reductive than in the oxidative half-reaction. This was confirmed by the $k_{cat}/K_{m(Al)}$ and reduction constants that are 2−3 orders of magnitude decreased for the His546 variants and up to 5 orders for the His502 variants, while the corresponding O_2 constants only decreased up to 1 order of magnitude. These results confirm His502 as the catalytic base in the AAO reductive half-reaction. The solvent kinetic isotope effect (KIE) revealed that hydroxyl proton abstraction is partially limiting the reaction, while the α-deuterated alcohol KIE showed a stereoselective hydride transfer. Concerning the oxidative half-reaction, directed mutagenesis and computational simulations indicate that only His502 is involved. Quantum mechanical/molecular mechanical (QM/MM) reveals an initial partial electron transfer from the reduced $FADH^-$ to O_2, without formation of a flavin-hydroperoxide intermediate. Reaction follows with a nearly barrierless His502H$^+$ proton transfer that decreases the triplet/singlet gap. Spin inversion and second electron transfer, concomitant with a slower proton transfer from flavin N5, yields H_2O_2. No solvent KIE was found for O_2 reduction confirming that the His502 proton transfer does not limit the oxidative half-reaction. However, the small KIE on $k_{cat}/K_{m(Ox)}$, during steady-state oxidation of α-deuterated alcohol, suggests that the second proton transfer from N5H is partially limiting, as predicted by the QM/MM simulations.
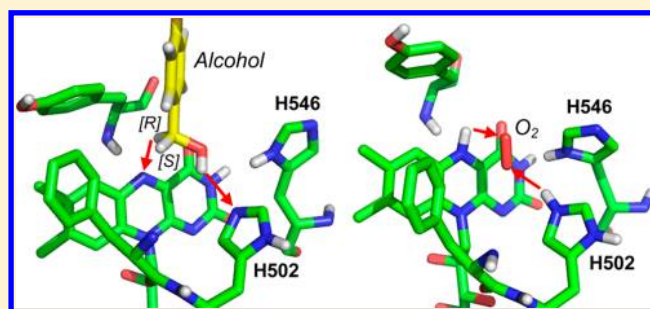
Fungal aryl-alcohol oxidase (AAO, EC 1.1.3.7) catalyzes the two-electron oxidation of aromatic, and aliphatic poly-unsaturated, primary alcohols to their corresponding aldehydes and simultaneously reduces O_2 to H_2O_2.[1] The extracellular H_2O_2 produced is required for lignin degradation as the oxidizing substrate for high-redox potential ligninolytic peroxidases.[2] Lignin removal is a key step for carbon recycling in land ecosystems and also a key issue for the industrial use of plant biomass in lignocellulose biorefineries, where biotechnology will contribute to the sustainable production of biofuels, chemicals, and other products.[3]

After gene cloning and homology modeling, the *Pleurotus eryngii* AAO was classified in the glucose-methanol-choline oxidase (GMC) superfamily of oxidoreductases due to common sequence and structural features.[4,5] These include the presence of two conserved active-site residues at catalytically relevant positions right in the vicinity of the FAD cofactor,

as reported in the crystal structures of these FAD-containing enzymes,[6−10] and confirmed later in the AAO crystal structure.[11] The conserved residues are a His-His pair, as in AAO and glucose oxidase (Figure 1A,B), or a His-Asn pair, as in pyranose 2-oxidase, cholesterol oxidase, choline oxidase, and cellobiose dehydrogenase (Figure 1C−F). Although a crystal structure is not available, a His-Asn pair (His567 and Asn616) is also predicted in methanol oxidase.[12]

Flavoenzyme catalytic cycles include two half-reactions corresponding to the successive reduction and oxidation of the flavin cofactor. The mostly accepted mechanism for the GMC reductive half-reaction starts with a substrate hydroxyl proton abstracted by an active-site base, followed by hydride
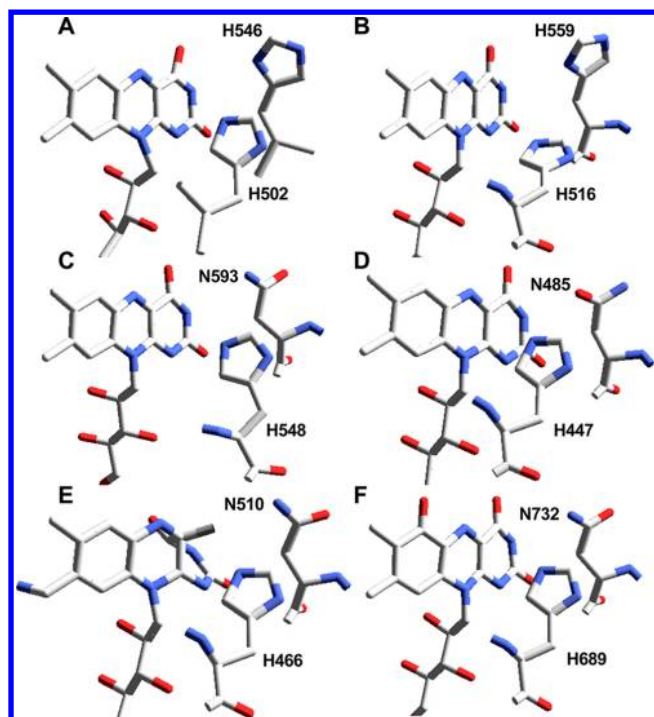
Figure 1. Active site His-His and His-Asn pairs in crystal structures of GMC flavooxidases. (A) *P. eryngii* AAO.[11] (B) *Aspergillus niger* glucose oxidase.[6] (C) *Trametes ochracea* pyranose 2-oxidase.[7] (D) *Brevibacterium sterolium* cholesterol oxidase.[8] (E) *Arthrobacter globiformis* choline oxidase.[9] (F) *Phanerochaete chrysosporium* cellobiose dehydrogenase (flavin domain).[10] Note the unusual bending of the flavin ring (and methyl-8 bond to protein) in choline oxidase (E). From PDB entries 3FIM, 1CF3, 1TTO, 1COY, 2JBV, and 1KGD, respectively.

abstraction by the quinonic flavin.[13] Mutational studies on the His-His and His-Asn pairs have aimed to address the catalytic role of these residues in substrate oxidation by different members of the GMC superfamily including AAO.[14−21]

The mechanism and the residues involved in the oxidative half-reaction, where O_2 is reduced to H_2O_2 by the flavin hydroquinonic form, are still to be completely understood although the main aspects have already been discussed.[22−25] It is generally accepted that the first step in flavin reoxidation is a single electron transfer from flavin to O_2 yielding a radical pair formed by the resulting superoxide anion and flavin semiquinone. Transient semiquinone has been detected in some flavooxidases,[26] but not in AAO even when one-electron photoreduction was tried.[1] The above pair can collapse on the flavin C4a atom to form a flavin-hydroperoxide intermediate, which participates in oxygen transfer reactions, or decomposes generating H_2O_2 and reoxidized flavin. Alternatively, the second electron can be transferred from the flavin semiquinone to the superoxide anion directly yielding H_2O_2 and oxidized flavin. The ability to stabilize the C4a-hydroperoxide intermediate, being rare in oxidases but present in monooxygenases, defines the different O_2 reactivity between both types of flavoenzymes.

In the present study we compare the role of the two conserved active-site residues of *P. eryngii* AAO (His502 and His546) to discriminate their contributions to both the reductive and oxidative half-reactions, with special emphasis on the latter one, by a combination of experimental and computational tools. Among them, site-directed mutagenesis followed by steady and transient-state kinetics helped to quantify the histidine involvement in catalysis, while substrate

and solvent kinetic isotope effects (KIE) informed the limiting steps in the two half-reactions. Finally, quantum mechanical/molecular mechanical (QM/MM) calculations contributed to explain the reaction mechanisms in energetic terms, and the eventual formation of intermediate species.

■ MATERIALS AND METHODS

Production of AAO and Mutated Variants. Native (wild-type) AAO of *P. eryngii* was obtained by *Escherichia coli* expression of the mature AAO cDNA (GenBank AF064069) followed by *in vitro* activation.[27] Mutated variants were prepared using the QuikChange site-directed mutagenesis kit (Stratagene). For mutagenic PCR, the cDNA cloned into the pFLAG1 vector was used as template, and the following oligonucleotides (direct sequences) bearing mutations (underlined) at the corresponding triplets (bold) as primers: (i) H502S, 5′-GCCAACACGATTTTC**AGC**CCAGTTGGAACGGCC-3′; (ii) H502A, 5′-GCCAACACGATTTTC**GCC**CCAGTTGGAACGGCC-3′; (iii) H546S, 5′-CCCTTCGCGCCCAACGCA**AGT**ACCCAAGGACCG-3′; and (iv) H546A, 5′-CCCTTCGCGCCCAACGCA**GCT**ACCCAAGGACCG-3′. Mutations were confirmed by sequencing (GS-FLX sequencer from Roche) and the mutated variants were obtained as described for recombinant AAO. Enzyme concentrations were determined using the molar absorbances of AAO and its H546S, H546A, H502A, and H502S variants (ε_{463} 11050 and 12400 $M^{-1} \cdot cm^{-1}$, ε_{467} 9669 and 9800 $M^{-1} \cdot cm^{-1}$, and ε_{468} 9980 $M^{-1} \cdot cm^{-1}$, respectively) calculated by heat denaturation and estimation of the free FAD (ε_{450} 11300 $M^{-1} \cdot cm^{-1}$) released.[28]

Steady-State Kinetics and pH Dependence. AAO activity was estimated spectrophotometrically by oxidation of *p*-methoxybenzyl alcohol (from Sigma-Aldrich) to the corresponding aldehyde (ε_{285} 16950 $M^{-1} \cdot cm^{-1}$).[1]

Steady-state kinetic constants for native AAO and its H546S and H546A variants were determined in bisubstrate kinetics, where the concentrations of alcohol (4−2000 μM) and O_2 (51, 128, 273, 566, and 1279 μM after bubbling buffer with different O_2/N_2 mixtures for 15 min) were simultaneously varied in 0.1 M phosphate, pH 6, at 25 °C, by extrapolation to saturation conditions. The constants were obtained by fitting (using Sigmaplot v.11) the initial rates to eq 1,[29] where e represents the enzyme concentration; k_{cat} is the maximal turnover; S is the concentration of alcohol; B is the concentration of O_2; $K_{m(Al)}$ and $K_{m(Ox)}$ are the Michaelis constants of alcohol and O_2, respectively; and K_d is the alcohol dissociation constant.

$$\frac{v}{e} = \frac{k_{cat}SB}{K_{m(Ox)}S + K_{m(Al)}B + SB + K_dK_{m(Ox)}} \quad (1)$$

Steady-state kinetic constants for the H502S and H502A variants were investigated varying only the alcohol concentration (62−5000 μM) in air-saturated buffer under the above conditions, since the low enzyme turnover rates for these variants were independent of O_2 concentration. The constants were obtained by fitting the initial rate data to the Michaelis−Menten equation.

The pH 3 to 9 dependence of activity of the mutated variants was estimated in 0.1 M buffer (citrate phosphate for pH 3−7.5, and pyrophosphate for pH 8−9) at 25 °C, under air atmosphere. Additionally, for native AAO and its H546S variant, pH dependence was also investigated in bisubstrate kinetics, as described above. The pH dependence of the kinetic constants was determined by fitting initial rates to eqs 2−4.

Data showing a slope (on a logarithmic plot) of +1 and −1 were fit to eqs 2 and 3, where pK_{a1} and pK_{a2} represent the pK_a values of the acid and basic residues, respectively. Data for bell-shaped pH profile were fitted to eq 4. In all equations, C is the pH-independent value of the kinetic parameter of interest.

$$log\ Y = log\left(\frac{C}{1 + \frac{10^{-pH}}{10^{-pK_{a1}}}}\right) \qquad (2)$$

$$log\ Y = log\left(\frac{C}{1 + \frac{10^{-pK_{a2}}}{10^{-pH}}}\right) \qquad (3)$$

$$log\ Y = log\left(\frac{C}{1 + \frac{10^{-pH}}{10^{-pK_{a1}}} + \frac{10^{-pK_{a2}}}{10^{-pH}}}\right) \qquad (4)$$

KIE on Steady-State Constants. Substrate KIE for AAO turnover (k_{cat}), $k_{cat}/K_{m(Al)}$, and $k_{cat}/K_{m(Ox)}$ was investigated using the α-dideuterated and the (R) and (S) α-monodeuterated enantiomers of p-methoxybenzyl alcohol (in the pH independent region of the AAO activity profile). The deuterated substrates, with 96% enantiomeric excess, were synthesized as previously described.[30] For solvent KIE investigation, the reaction components were dissolved in deuterated 0.1 M phosphate, p^2H 5.6 (pH 6) after exhaustive AAO dialysis against deuterated buffer. The KIE values were obtained by comparing the kinetic constants determined in H_2O with those determined in ^2H_2O buffer (using α-protiated alcohol). Solvent viscosity effect was investigated using 30% (w/v) glycerol and calculated by comparing the constants obtained in the absence and in the presence of the viscogen. Multiple KIE values were calculated by comparing the kinetic constants on α-protiated p-methoxybenzyl alcohol in H_2O buffer with those on α-deuterated p-methoxybenzyl alcohol in ^2H_2O buffer.

First the substrate, solvent, and multiple KIE values for apparent kinetic constants at each of nine p-methoxybenzyl alcohol concentrations (or five O_2 concentrations) were estimated by varying the O_2 (or alcohol) concentration (using eq S1 from Supporting Information). Then, the same KIE values were estimated at substrate-saturating conditions (from bisubstrate kinetics) as the ratio between the kinetic constants on α-protiated with respect to α-deuterated p-methoxybenzyl alcohol, determined using eq 1.

Stopped-Flow Measurements: Enzyme Turnover and Transient-State Kinetics. An Applied Photophysics SX18.MV stopped-flow spectrophotometer, interfaced with an Acorn computer, was used, and data were processed with the SX18.MV and Xscan softwares for experiments with single-wavelength and diode-array detectors, respectively.

For enzyme-monitored turnover experiments,[29] air-saturated AAO and its H502S, H502A, and His546A variants (H546S was too unstable for stopped-flow experiments) and substrate solutions were mixed in the stopped-flow cell, and evolution of the redox state of the FAD cofactor was monitored at the flavin maximum observed in the 462−467 nm range (flavin-I band) for native AAO and its variants.

The reductive half-reaction was studied under anaerobic conditions.[29] Tonometers containing enzyme and substrate solutions were made anaerobic by successive evacuation and flushing with argon. These solutions also contained glucose (10 mM) and glucose oxidase (10 $U \cdot mL^{-1}$) to ensure anaerobiosis. Drive syringes in the stopped-flow apparatus were made anaerobic by sequentially passing a sodium dithionite solution and O_2-free buffer. Measurements were carried out in 0.1 M phosphate, pH 6, at 25 °C for the H502S, H502A, and H546A variants, and at 12 °C for native AAO due to its extremely rapid reduction. Spectral evolution was studied by global analysis and numerical integration methods using the Pro-K software (Applied Photophysics Ltd.) and data were fitted to one ($A \rightarrow B$) or two step ($A \rightarrow B \rightarrow C$) models ($A$, B, and C are spectral species reflecting a distribution of enzyme intermediates at a certain point along the reaction and do not necessarily represent a single distinct enzyme intermediate). The observed rate constants (k_{obs}) at different substrate concentrations (S) were fitted to eq 6, where k_{red} and K_d are the flavin reduction and dissociation constants, respectively.

$$k_{obs} = \frac{k_{red}S}{K_d + S} \qquad (6)$$

The rate constants for flavin reoxidation were measured by monitoring the increase of the flavin-I band after mixing (at 12 °C) the reduced enzyme, in anaerobic 0.1 M phosphate (pH 6), with the same buffer equilibrated at different O_2 concentrations. Previously, the enzyme samples were reduced under anaerobic conditions, using a modified tonometer with a side arm containing a solution of p-methoxybenzyl alcohol (final 1.2:1.0 molar excess). The spectral evolution data for the oxidative half-reaction were fitted to one or two step models. The flavin reoxidation constant was obtained from eq 7, where $k_{obs(app)}$ is the apparent observed rate constant associated with flavin reoxidation at any given concentration of O_2, and $k_{ox(app)}$ is the apparent second-order rate constant for reoxidation.

$$k_{obs(app)} = k_{ox(app)}[O_2] \qquad (7)$$

System Set-Up for Computational Studies. The AAO coordinates for simulation of the O_2 reduction reaction were taken from the crystal structure in PDB entry 3FIM[11] and processed with the protein preparation wizard available in Maestro.[31] This algorithm builds hydrogen-bonded clusters and performs 100000 Monte Carlo moves by reorienting hydroxyl and thiol groups, water molecules, amide groups of asparagines and glutamines, and the imidazole ring in histidines. The algorithm also predicts protonation states. Each possibility is scored based on the total number of hydrogen bonds and their quality (relative to an idealized hydrogen bond). In particular, all aspartic, glutamic, lysine, and arginine residues were kept in their charged states. His190 and His546 were δ-protonated, His91, His313, His387, and His398 were ε-protonated and His137, His148, His360, and His502 were fully protonated. The two ligands, O_2 and p-methoxybenzyl alcohol, were diffused to the active site using PELE,[32] with results published elsewhere.[21,33] The initial structure for the oxidative half-reaction QM/MM calculations, described below, was taken from one of these trajectories after modifying p-methoxybenzyl alcohol to the p-methoxybenzaldehyde (p-anisaldehyde) product and the FAD molecule to its anionic reduced form (FADH$^-$, proton in N5 with N1 deprotonated). Then a solvation layer was added by running a short molecular dynamics trajectory (see Supporting Information). After solvent equilibration in a periodic box, the layer was obtained by removing all water molecules and ions beyond 8 Å from the

Table 1. Steady-State Kinetic Constants for Alcohol and O$_2$ Substrates During p-Methoxybenzyl Alcohol Oxidation by Native AAO and its Site-Directed Variants[a]

	k_{cat} (s^{-1})	$K_{m(Al)}$ (μM)	$k_{cat}/K_{m(Al)}$ (s$^{-1}\cdot$mM^{-1})	$K_{m(Ox)}$ (μM)	$k_{cat}/K_{m(Ox)}$ (s$^{-1}\cdot$mM^{-1})
AAO	197 ± 2	49 ± 1	3980 ± 110	159 ± 5	1240 ± 40
H502S	0.069 ± 0.005	1290 ± 250	0.054 ± 0.010	(~1)[b]	nd[c]
H502A	0.072 ± 0.002	3820 ± 230	0.019 ± 0.001	(<1)[b]	nd
H546S	16.6 ± 1.4	310 ± 60	53 ± 11	18 ± 3	923 ± 149
H546A	3.5 ± 0.1	1160 ± 30	3.0 ± 0.1	6 ± 1	590 ± 103
F501A[d]	66 ± 2	265 ± 8	250 ± 9	3880 ± 120	17 ± 1

[a]Steady-state constants were determined from bisubstrate kinetics, where the concentration of both substrates (alcohol and O$_2$) were simultaneously varied in 0.1 M phosphate, pH 6, at 25 °C. [b]The $K_{m(Ox)}$ values in parentheses are rough estimations based on the reoxidation apparent constants from Table 2 (see footnote c). [c]nd, not determined because of no O$_2$ dependence. [d]Adapted from Hernández-Ortega et al.[33] Means and standard errors are provided.

Table 2. Transient-State Kinetic Constants for Native AAO and its Site-Directed Variants Reduction by p-Methoxybenzyl Alcohol and Reoxidation by O$_2$[a]

	reduction			reoxidation	
	k_{red} (s^{-1})	K_d (μM)	$k_{red(app)}$ (s$^{-1}\cdot$mM^{-1})	$k_{ox(app)1}$ (s$^{-1}\cdot$mM^{-1})	$k_{ox(app)2}$ (s$^{-1}\cdot$mM^{-1})
AAO	139 ± 16	26 ± 5	5350 ± 1200	657 ± 24	nd[b]
H502S	0.111 ± 0.002	4740 ± 180	0.023 ± 0.001	56 ± 1	18 ± 2
H502A	0.076 ± 0.001	3180 ± 70	0.024 ± 0.001	115 ± 1	8 ± 1
H546A	3.96 ± 0.01	1310 ± 30	3.03 ± 0.07	491 ± 8	nd
F501A[c]	35 ± 5	153 ± 2	229 ± 33	8 ± 1	no[d]

[a]Transient-state constants for AAO reduction by alcohol (including first-order rate constants and apparent second-order rate constant) and reoxidation by O$_2$ (only apparent second-order rate constant), the latter including two constants ($k_{ox(app)1}$ and $k_{ox(app)2}$) corresponding to the fast (A → B) and slow (B → C) steps, respectively (see Figure 4), were determined in 0.1 M phosphate, pH 6, at 12 °C. [b]nd, not determined because of no O$_2$ dependence. [c]From Hernández-Ortega et al.[33] [d]no, not determined because no second step was observed. Means and standard errors are provided.

protein surface. In the case of the QM calculations the protein environment was removed leaving the active site groups: flavin, His502, and the O$_2$ molecule. Two models were investigated, where in the smallest of these only the flavin and the O$_2$ were used.

QM Simulations. The QM calculations were performed with Jaguar.[34] For two different size systems, one comprising an FAD molecule (truncated beyond the N10 atom) and an O$_2$ molecule and another with a histidine residue added, we constructed several geometry optimizations and reaction coordinates in the singlet and triplet spin states using the unrestricted density functional M06.[35] Tests with different basis sets,[36] 6-31G(d,p), 6-311G(d,p), and 6-311G(3df,3pd)++ (the latter including only single point calculations), indicate that the geometries are fairly insensitive to the basis set employed, with differences in energy within the error of the method (see Table S1 in Supporting Information). Therefore, the 6-311G** basis set was used in all the optimizations.

QM/MM Simulations. The QM/MM calculations were performed with the Qsite software,[37] and all structures were optimized at the M06/6-311G(d,p)/OPLS level. Full optimizations were performed within the quantum region plus 10 Å layer of MM atoms (beyond this point they were kept frozen). A nonbounded cutoff of 50 Å was used to ensure a correct MM point charge polarization of the QM region. Once the structures were optimized, point charges were localized at each atomic center and derived from the electrostatic potential (ESP). These charges were then used to assess the amount of electron transfer along the different stationary points.

Geometry optimizations and reaction coordinates were done for a set of systems where the quantum region was progressively increased. The smallest system is similar to the

one used in the QM calculations, where the truncated FAD and O$_2$ molecules are included. In addition, four more systems were investigated, where different residues/molecules were progressively added: (i) His502; (ii) His546; (iii) His313 and Glu389; and (iv) p-anisaldehyde. In this way a set of five systems was prepared with a total of 33, 45, 56, 77, and 95 atoms in the quantum region. Additionally, two more systems were investigated, where the H502A and H546A mutations were introduced to the largest of the previous regions (iv).

■ **RESULTS**

Production and Spectral Properties of Histidine Variants. The H502S, H502A, H546S, and H546A mutations were introduced by PCR on the mature AAO codifying sequence, which was expressed in *E. coli*. The corresponding variants were purified to homogeneity after *in vitro* refolding and cofactor incorporation, showing a A_{280}/A_{463} ratio ~10, similar to that found for the native enzyme (His → Arg variants were also tried but they could not be *in vitro* activated). The UV−visible spectra of the variants (Supporting Figure S1) show the typical flavin-I band around 465 nm indicating that the cofactor is incorporated (in the oxidized state). The spectrum of the H546S variant is similar to that of native AAO, with maxima at 387 and 463 nm. However, the maxima of the H502S, H502A, and H546A variants are situated at 390 and 467 nm, with a displaced shoulder at 498 and 494 nm for the H502S/A and H546A variants, respectively (compared with the 474 nm shoulder of native AAO), revealing a slight alteration of the flavin environment.

Alcohol and O$_2$ Steady-State Kinetics Constants. Table 1 shows the steady-state kinetic constants from bisubstrate kinetics of native AAO and the four histidine variants. Tables 1

and 2 also provide the previously reported kinetic constants for the F501A variant,[33] which are discussed later. The H502S and H502A mutations cause a strong decrease in turnover (around 2800 fold), while the H546S and H546A mutations result in more modest decreases (10 and 50 fold, respectively). All the substitutions also cause an increase in the K_m for the alcohol, which was larger for the H502S and H502A variants (27- and 80-fold increases, respectively) than for the H546S and H546A variants (7- and 25-fold increases, respectively). The above changes make the H546S, H546A, H502S, and H502A variants 75-, 1330-, 73700-, and 199000-fold less efficient, respectively, than native AAO oxidizing p-methoxybenzyl alcohol, as shown by the $k_{cat}/K_{m(Al)}$ values.

The His502 variants exhibit no O_2 dependence for alcohol oxidation under steady-state conditions. Therefore, their reactivity with O_2 can be determined only under transient-state conditions, as described below. In contrast, the O_2 reactivity of the His546 variants can be estimated under steady-state conditions yielding, respectively, $K_{m(Ox)}$ values 9- and 26-fold lower than native AAO, although they are ~1.3- and 2-fold less efficient reducing O_2, respectively. This higher apparent affinity for O_2 is related to a higher contribution of the oxidative half-reaction to turnover, as described below.

pH Dependence of AAO Activity. The pH dependence of the steady-state constants for alcohol oxidation by AAO and its four histidine variants was investigated under air atmosphere (yielding apparent constant values) as a continuation of previous studies where only the H502S and H546S variants had been investigated.[21] As previously reported,[29] native AAO does not show a pH dependence for p-methoxybenzyl alcohol oxidation, maybe due to H-bonding of active-site histidines with the alcohol,[30] pushing the pK_a outside the achievable pH range. For the two His502 variants, their extremely low activity (see Table 1) prevents detection of a pH effect on the $k_{cat(app)}/K_{m(Al)(app)}$, and only the pH effect on $k_{cat(app)}$ can be observed (Figure 2A). The activity of these two variants is stable in the range of pH 3−6 and slightly decreased at more basic values, suggesting the presence of a residue that must be protonated for turnover.

Replacement of His546 resulted in a more clearly observable effect of pH on the oxidation of p-methoxybenzyl alcohol. The $k_{cat(app)}$ of the two His546 variants gave a bell-shaped profile at the different pH values (Figure 2A) that is consistent with the involvement of two ionizable groups at the active site. One group with an acidic pK_a must be unprotonated for turnover, and a second group with a basic pK_a must be protonated. Additional information on the residue(s) specifically involved in alcohol oxidation was provided by the effect of pH on the $k_{cat(app)}/K_{m(Al)(app)}$ of the two His546 variants. The profiles obtained (Figure 2B) show a residue in the free enzyme with a pK_a ~3.8 that must be unprotonated for alcohol oxidation.

Although it had been previously reported that $k_{cat}/K_{m(Ox)}$ of native AAO was pH independent,[29] a slight decrease was observed at the highest pH values (as illustrated in Supporting Figure S2). Unfortunately, no pH profiles enabling pK_a calculation could be obtained for the $k_{cat}/K_{m(Ox)}$ values of the His502 and His546 variants due to the very low $K_{m(Ox)}$ values obtained (that in the case of the His502 variants prevented $k_{cat}/K_{m(Ox)}$ determination as mentioned above).

Enzyme-Monitored Turnover: Changes in the Flavin Redox State. To identify the redox state of the cofactor during catalysis, native AAO and its H502S, H502A, and H546A variants (H546S was too unstable for these experiments) were
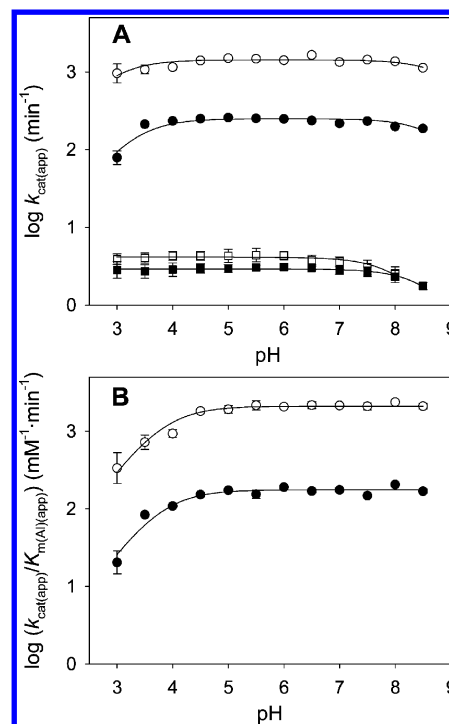

Figure 2. pH dependence of the steady-state kinetic constants for p-methoxybenzyl alcohol oxidation by the His502 and His546 variants. (A) Dependence of $k_{cat(app)}$ for H502A (■; pK_a 8.7 ± 0.1), H502S (□; pK_a 8.1 ± 0.1), H546A (●; pK_{a1} 3.2 ± 0.1, and pK_{a2} 8.9 ± 0.2), and H546S (○; pK_{a1} 2.8 ± 0.1, and pK_{a2} 9.0 ± 0.1). (B) Dependence of $k_{cat(app)}/K_{m(Al)(app)}$ for H546A (●; pK_a 3.8 ± 0.1) and H546S (○; pK_a 3.8 ± 0.1). The errors considered in the measured parameters were taken larger than the standard deviation between three replicates and the numerical errors after fitting analysis. All reactions were performed in 0.1 M citrate-phosphate at 25 °C under air atmosphere, enabling calculation of k_{cat} values for the His502 variants, but only apparent $k_{cat(app)}$ values for the His546 variants.

mixed in the stopped-flow instrument with saturating concentrations of p-methoxybenzyl alcohol under air, and the spectral changes produced were followed (as illustrated in Supporting Figure S3). The evolution of the redox state of the enzyme and its variants under these conditions, as revealed by changes in the intensity of the flavin-I band, is shown in Figure 3.

For native AAO, a fast decrease in absorbance is observed within the first milliseconds, before attaining a short steady-state period (~10−80 ms) where ~80% of the enzyme is in the oxidized form. However, for the histidine variants the initial absorbance is stable (H546A) or even increased (H502S and H502A) after mixing. These increases are produced when high alcohol concentrations are used for enzyme saturation and are due to enzyme−substrate complex formation, as reported also for aldehyde oxidation by AAO.[38] Moreover, the steady-state period (characterized by stable 467 nm absorbance) is much longer (10−300 s) than for native AAO, and the variants are fully oxidized during the whole period. In all the cases the enzymes are finally reduced due to O_2 depletion in the solution.

The spectral evolution during AAO turnover with p-methoxybenzyl alcohol suggests formation of a charge-transfer complex with a broad band centered around 550 nm (Supporting Figure S3A) as described for other flavoproteins.[39] This charge-transfer complex is absent from the turnover spectra of the H502S, H502A, and H546A variants (Figure
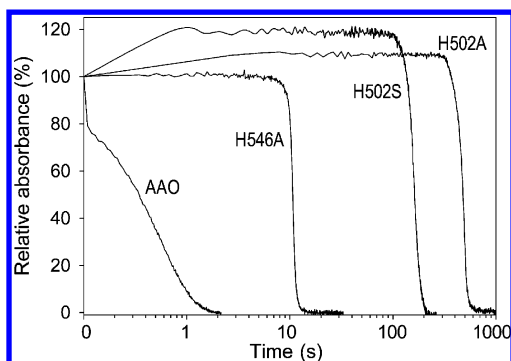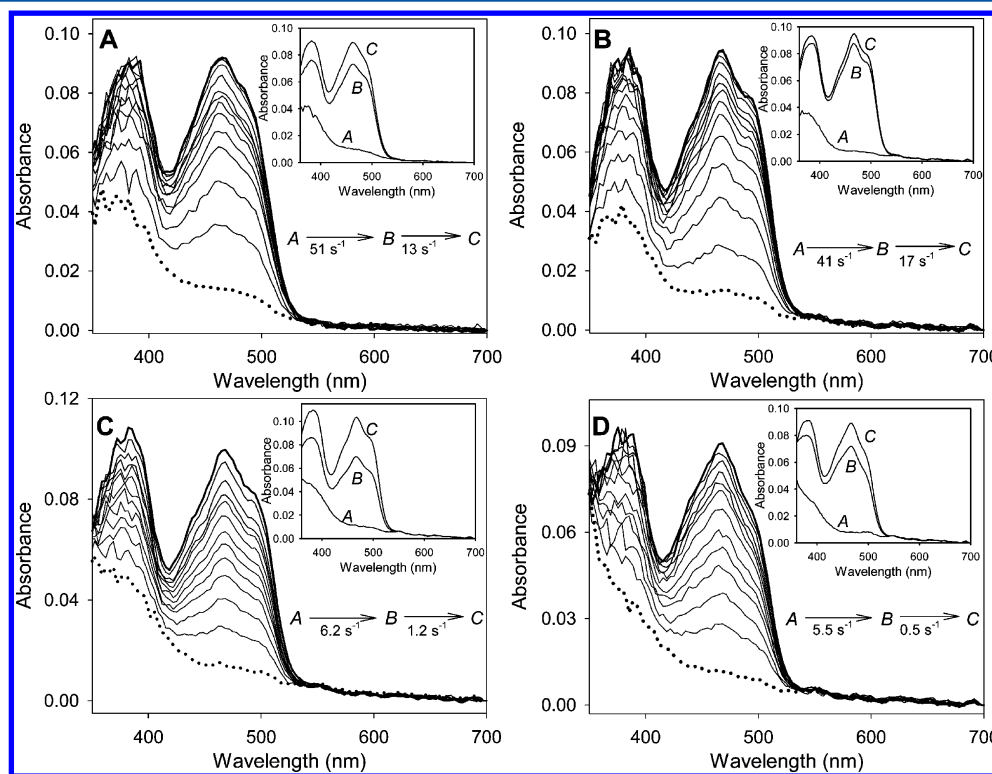
Figure 3. Redox state of AAO and its His546 and His502 variants during turnover. The percentage of oxidized FAD cofactor during turnover (illustrated in Supporting Figure S3) was monitored at the flavin-I band wavelength (462 nm for native AAO, and 467 nm for its variants) and shown using a logarithmic time scale. Measurements were performed in the stopped-flow instrument using an aerobic solution of enzyme (∼10 μM) and saturating *p*-methoxybenzyl alcohol concentrations (1, 2, 9, and 9 mM in A−D, respectively), in 0.1 M citrate-phosphate, pH 6, at 25 °C (final concentrations).

S3B−D) suggesting that substrate accommodation is affected by these active-site mutations.

Reductive Half-Reaction. The reductive half-reaction of the native AAO and its H502S, H502A, and H546A variants was investigated by anaerobic stopped-flow spectrophotometry. The spectra obtained indicated full reduction of AAO in all cases (Supporting Figure S4). Interestingly, the anaerobic

conditions used prevented formation of the charge-transfer complex found during AAO turnover, implying that O_2 is involved. Global analysis of the spectral evolution during AAO reduction best fit to a two step model (where the $A \rightarrow B$ step is very fast, and the $B \rightarrow C$ step is concentration independent and too slow for being catalytically relevant), while the H502S, H502A, and H546A reduction better fit to a single step model (with very slow reduction rates). The observed rates (k_{obs}) for the fast ($A \rightarrow B$) reaction of native AAO show hyperbolic dependence on the alcohol concentration, allowing constant determination for AAO reduction (k_{red}) and substrate dissociation (K_d) (Table 2). These values are in agreement with the steady-state K_m and k_{cat} values, confirming that the reductive half-reaction is the rate limiting step in AAO catalysis. The same transient-state kinetic constants can also be obtained for the one-step reduction of the AAO variants (Table 2). The k_{red} values for the H546A, H502S, and H502A variants are at least 35-, 1250-, and 1830-fold lower, respectively, than those of native AAO (the latter estimated at 12 °C). A strong alcohol affinity decrease (50−200 fold higher K_d values) is also observed.

Oxidative Half-Reaction. The oxidative half-reaction of the native AAO and its H502S, H502A, and H546A variants was also investigated by stopped-flow spectrophotometry. As shown in Figure 4, oxidation of flavin hydroquinone to the fully oxidized quinonic state best fit to a two step model in all the cases. For native AAO and the H546A variant the $A \rightarrow B$ step is fast and O_2 dependent, and the $B \rightarrow C$ step is slower and O_2 independent, while for the H502S and H502A variants both the

Figure 4. Spectral changes during oxidation of AAO and its His546 and His502 variants by O_2. (A and B) Spectra of native AAO and H546A variant, respectively, at 2, 9, 17, 24, 32, 40, 47, 55, 63, 70, 93, 125, 150, and 175 ms. (C) H502S spectra at 9, 60, 112, 163, 214, 265, 316, 419, 520, 620, 830, 1230, and 1650 ms. (D) H502A spectra at 9, 60, 112, 163, 214, 265, 370, 520, 620, 830, 1650, 2470, and 3900 ms. The first and last above spectra are shown as dotted and thick lines, respectively. Spectra were recorded after mixing reduced enzyme (∼9 μM) with 0.1 M phosphate, pH 6, containing 75 μM O_2 in the stopped-flow instruments at 12 °C (final concentrations). The insets show the simulated spectral species predicted by globally fitting the experimental data to a two step ($A \rightarrow B \rightarrow C$) model.

fast ($A \rightarrow B$) and the slow ($B \rightarrow C$) steps are O_2 dependent, suggesting the existence of a different reoxidation mechanism for the His502 variants (including two O_2-dependent processes). Rate constants for flavin reoxidation were estimated from absorbance increases at different O_2 concentrations. In all cases, the k_{obs} for the fast ($A \rightarrow B$) step, when plotted as a function of O_2 concentration, define second-order processes (Supporting Figure S5). The same is observed when the second step ($B \rightarrow C$) was O_2 dependent (His502 variants). In this way, the reoxidation constants for the fast ($k_{ox(app)1}$) and slow steps ($k_{ox(app)2}$) were obtained (Table 2), although the latter only for the His502 variants. The $k_{ox(app)}$ for the H546A variant is 1.3-fold lower than that of native AAO, while the $k_{ox(app)1}$ values for the H502S and H502A variants are 12- and 6-fold lower, respectively, and the $k_{ox(app)2}$ values are always significantly lower.

Substrate and Solvent KIE on Steady-State Kinetic Constants. KIE values were first estimated on apparent kinetic constants ($k_{cat(app)}$ and $k_{cat(app)}/K_{m(Ox)(app)}$) at nine concentrations of α-dideuterated ($^2H_2$) and α-monodeuterated (R-^2H and S-^2H) p-methoxybenzyl alcohol (in H_2O buffer) and multiple KIE on α-dideuterated alcohol kinetic constants in ^2H_2O buffer (compared with α-protiated alcohol in H_2O buffer) using five different O_2 concentrations (Supporting Table S2 and Figure S6A). A similar comparison has been reported for AAO substrate KIE values at different O_2 concentrations[30] (and the comparison of multiple KIE values is included here for the first time; Supporting Figure S6B). In both cases, the KIE on $k_{cat(app)}$ (for each alcohol or O_2 concentration) increases to attain saturation conditions (while the $k_{cat(app)}/K_{m(Ox)(app)}$ KIE values are higher at the lowest alcohol concentrations).

To approach the value of the true isotope effect, KIE on k_{cat}, and both $k_{cat}/K_{m(Al)}$ and $k_{cat}/K_{m(Ox)}$, was estimated at substrate-saturating conditions (Table 3). The highest KIE value

Table 3. Steady-State Substrate, Solvent and Multiple KIE and Viscosity Effect on AAO k_{cat}, $k_{cat}/K_{m(Al)}$, and $k_{cat}/K_{m(Ox)}$[a]

	kinetic isotope and viscosity effects on:		
	k_{cat}	$k_{cat}/K_{m(Al)}$	$k_{cat}/K_{m(Ox)}$
(R)-[α-^2H]-p-methoxybenzyl (H_2O)	5.18 ± 0.09	3.59 ± 0.12	1.53 ± 0.06
(S)-[α-^2H]-p-methoxybenzyl (H_2O)	1.37 ± 0.02	1.25 ± 0.05	1.15 ± 0.05
[α-$^2H_2$]-p-methoxybenzyl (H_2O)	7.87 ± 0.09	3.91 ± 0.13	1.57 ± 0.06
solvent KIE (^2H_2O)	1.49 ± 0.02	1.59 ± 0.08	1.07 ± 0.05
[α-$^2H_2$]-p-methoxybenzyl (^2H_2O)	10.60 ± 0.10	4.84 ± 0.22	1.45 ± 0.07
viscosity effect (30% glycerol)	0.99 ± 0.01	1.03 ± 0.04	1.01 ± 0.04

[a]Substrate and solvent KIE values are the ratio between the activities on α-protiated with respect to α-deuterated p-methoxybenzyl alcohols, or on α-protiated alcohol in H_2O buffer (pH 6.0) with respect to ^2H_2O buffer (p^2H 5.6), respectively. The multiple KIE is the ratio between the activity in α-protiated alcohol in H_2O buffer and α-dideuterated alcohol in ^2H_2O buffer. The viscosity effect is the ratio between the activities with α-protiated alcohol in normal with respect to glycerol-containing buffer. All the KIE values for steady-state constants were experimentally determined from bisubstrate kinetics (the KIE values for the apparent constants at each of the nine O_2 concentrations assayed are included in Supporting Table S2). Means and standard errors are provided

corresponds to multiple KIE ($^{D,D_2O}(k_{cat})$) values over 10) when both dideuterated alcohol and deuterated buffer are compared with the protiated ones, followed by $^D(k_{cat})$ for the α-dideuterated and (R)-α-monodeuterated alcohol (5–8) confirming that alcohol α-deuteration strongly affects AAO catalysis. Moreover, the $^D(k_{cat}/K_{m(Al)})$ shows that the decrease observed is mainly due to the effect on alcohol oxidation by the enzyme, with α-dideuterated and (R)-α-monodeuterated values of 3.5–4.0, compared with only 1.2 for the (S) enantiomer, in agreement with previous studies showing AAO stereo-selectivity.[21,30] Interestingly, low but significant $^D(k_{cat}/K_{m(Ox)})$ values are also obtained when α-dideuterated and (R)-α-monodeuterated alcohol are used as enzyme reducing substrates (1.6 and 1.5, respectively). However, when the (S)-α-monodeuterated alcohol is used, which does not result in deuterium transfer to flavin N5 due to the stereoselective hydride transfer by AAO mentioned above, no KIE was observed.

Solvent KIE was investigated on AAO k_{cat}, $k_{cat}/K_{m(Al)}$, and $k_{cat}/K_{m(Ox)}$. The $^{D_2O}(k_{cat}/K_{m(Al)})$ and $^{D_2O}k_{cat}$ values obtained (1.5–1.6) and the absence of a viscosity effect (Table 3) indicate that abstraction of an exchangeable hydrogen (most probably the alcohol hydroxyl proton) by catalytic His502 is partially limiting alcohol oxidation by AAO.[21] However, no significant solvent KIE viscosity effect is detected on the $k_{cat}/K_{m(Ox)}$.

The above conclusions were confirmed by the multiple KIE values for $k_{cat}/K_{m(Al)}$ and $k_{cat}/K_{m(Ox)}$ (Table 3, and Supporting Figure S6A). As already reported,[21] the multiple KIE for $k_{cat}/K_{m(Al)}$ (~ 5) is near the product between the substrate and solvent KIE values, confirming the two individual effects. However, the multiple KIE on $k_{cat}/K_{m(Ox)}$ (~ 1.5) coincide with that observed with α-deuterated alcohol in H_2O buffer, confirming the absence of a significant solvent effect on the O_2 reaction. More interestingly, the latter result reveals that the ^2H replacement rate at the flavin N5 position during turnover (with R-^2H-labeled alcohol) is higher than the ^2H replacement by exchange with the deuterated solvent. This results in full N5^2H labeling under turnover conditions, even when the reaction with deuterated alcohol is performed in H_2O.

QM Calculations on O_2 Reaction with Flavin. O_2 reduction by flavin hydroquinone was first simulated by pure QM calculations including only O_2 and a reduced FAD (truncated at N10). Thus, only these two molecules without the enzymatic environment or solvent are included in this initial model. We began by investigating the existence of a flavin-hydroperoxide intermediate. Since O_2 reaction involves a triplet to singlet spin change, both spin states were investigated. In a free optimization (no geometric restrains) in the triplet state, the O_2 molecule remains parallel to the FAD ring about 2.8 Å away from C4a. Analysis of the electrostatic potential charges shows that 40% of the electron density was already transferred from the FAD moiety to O_2. The unrestrained optimization in the singlet state, however, produces a final compound with the O_2 molecule bounded at the C4a position (1.5 Å) and proton transfer from the N5 atom to the free oxygen atom. Here 85% of the electron density has already been displaced from the flavin molecule to the oxygen moiety. Figure 5A,B shows the fully optimized reactants and products in triplet and singlet states, respectively.

By restraining the oxygen to the unbound position in the singlet state, we could compute the triplet/singlet energy gap at the reactant configuration, ~ 22 kcal·mol^{-1} favorable for the
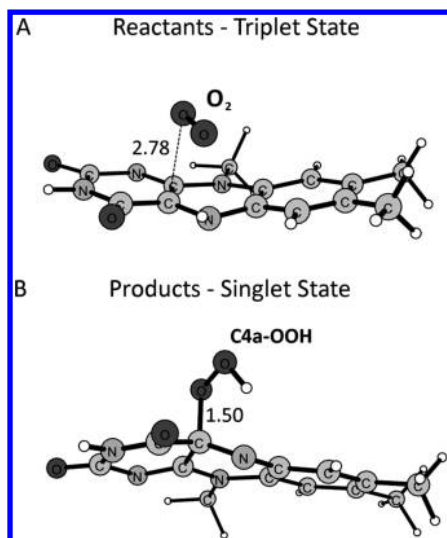
Figure 5. Pure QM optimization for the isolated model system constituted only the reduced flavin and O_2 molecule (FAD + O_2). In panel A the fully optimized reactants and in B the products, including C4a-hydroperoxide adduct, for O_2 reduction by free flavin. All distances displayed are in Å (the Cartesian coordinates for the main stationary points obtained are provided in Supporting Table S3A).

triplet, a similar value to the molecular oxygen spin inversion. The overall process, however, is 5.3 kcal·mol^{-1} exothermic (Table 4), indicating that for this QM model the flavin-hydroperoxide is formed (Figure 5B).

Table 4. Calculated Energies (kcal·mol^{-1}) and Spin Inversion Point (Distance from Flavin C4a, in Å) for O_2 Reduction for Different Systems Studied by QM and QM/MM^a

	QM	QM/MM		
	FAD + O_2	FAD + O_2	FAD + O_2 + H502	FAD + O_2 + H502 + H546
E1	21.7	14.2	10.0	11.1
E2	14.2	6.5	4.6	4.6
E3	−5.3	−11.2	−27.3	−24.7
inversion distance	1.98	2.16	2.19	2.19

^{a}E1, energy difference between the reactants in triplet and singlet states; E2, energy required by the reaction at the point where spin inversion occurs; and E3, energy difference between the triplet state reactants and the singlet state products.

The above results were calculated in the gas phase, but the triplet/singlet gap was also assessed in water (with a dielectric constant ~80) and in chloroform (with a dielectric constant, ~4, similar to the bulk protein environment). We found that the energy difference is considerably reduced in water (14.5 kcal·mol^{-1}), while the calculations in chloroform were similar to the gas phase (19.2 kcal·mol^{-1}).

Next we added a protonated histidine (modeled to be His502) into the QM model. In order to keep the relative orientation between the FAD molecule and this residue identical to the AAO active site disposition, a set of atomic coordinates were restrained (namely, CB, CG, CE1 from His502 and the three carbon atoms from the methyl groups in the flavin group). Thus, by adding this charged histidine the model has now a source for a second proton. The free

optimization in the singlet state drives the system spontaneously into formation of the products hydrogen peroxide and oxidized flavin, without formation of a flavin-hydroperoxide. The process involves first a proton transfer from His502 followed by the proton from the flavin N5. Interestingly, the triplet/singlet energy for the reactants structure is now reduced to 11 kcal·mol^{-1}.

QM/MM Calculations on O_2 Reaction with Flavin at the AAO Active Site. QM/MM calculations were used to predict the O_2 reduction reaction by flavin hydroquinone at the AAO active site. Hence, at this point the full enzyme plus a solvation layer was included. Five different quantum regions were employed. The first region, similar to the gas phase QM studies, was based only on the FAD and O_2, while the rest of the protein was kept in the MM region. Thus, this model only includes one proton capable of being transferred to the O_2 molecule (His502 not included in the quantum region). The reactant triplet state, similar to the QM results in the absence of the enzyme, presents the O_2 at a distance to C4a of 2.7 Å with 41% of electron density being transferred to O_2. Again, by restraining the oxygen we could compute the triplet/singlet energy gap, which in the presence of the enzyme is reduced to 14.2 kcal·mol^{-1}. Interestingly, when the singlet state is allowed to optimize freely addition to C4a by the O_2 molecule does not occur. Instead spontaneous proton transfer from flavin N5 atom takes place with the O−C4a distance approaching 2.2 Å where it remains loosely complexed, a 11.2 kcal·mol^{-1} exothermic process (Table 4).

As observed in the QM simulation, when His502 was included in the quantum region the singlet state optimization spontaneously led to H_2O_2, without intermediate addition to the C4a. The reaction proceeded with O_2 approximation to the N5−C4a locus, where it abstracted one proton from N5 and an additional proton from His502. As shown in Figure 6 (left), the exploration of the C4a-potential energy surface showed a reactant triplet/singlet energy gap of 10.0 kcal·mol^{-1} and an overall exothermicity of 27.3 kcal·mol^{-1} (Table 4). These values appear independent of the size of the quantum region, as confirmed by repeating the above calculation with the progressive increase of the quantum region. Therefore, even if the enzyme reduces considerably this gap, the energy profile along the O−C4 reaction coordinate still presents a significant barrier (left panel in Figure 6). The exploration of a possible proton transfer mechanism in the triplet state, however, introduces a more favorable path for the O_2 reduction.

First, the reaction coordinate for the N5 proton transfer in the triplet state proved to be unfavorable given the progressive increase in the potential energy surface (free optimization always yields the proton back at the flavin N5 atom). On the other hand, removal of the His502 proton reveals a 1.5 kcal·mol^{-1} activation barrier and a quasi-degenerate intermediate (depicted as "Int" in Figure 6, center). Taking into account the zero point energy corrections along the O−H coordinate (~2/3 kcal·mol^{-1}) this step should be barrierless. If we now compare the energy difference between the singlet and triplet states following the proton transfer from His502, we find that the gap is 3 kcal·mol^{-1} opposed to the 10 kcal·mol^{-1} gap previous to proton transfer. Following the spontaneous His502 proton transfer, N5 proton transfer still presents a progressive increase in the triplet potential energy. This time, however, we find a spin crossing point which is ~2 kcal·mol^{-1} above the triplet minima, from which the products are spontaneously produced leading to an overall exothermicity of 27.3 kcal·mol^{-1}
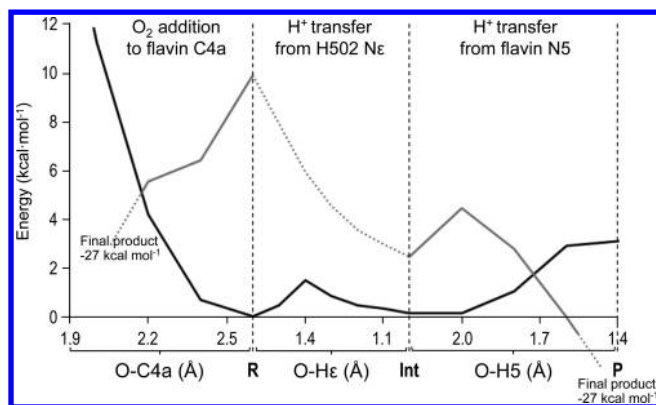
Figure 6. Potential energy curves for O_2 reduction by AAO computed with QM/MM for singlet (gray) and triplet (black) states. (Left) O_2 addition to the C4a center: the reaction coordinate is the distance between one of the O_2 atoms and the C4a of FAD; and the dotted line represents the full optimization of the products which lie 27 kcal·mol^{-1} below the reactants. (Center) Proton transfer from His502: the reaction coordinate is the distance between one oxygen atom of O_2 and the Nε proton of His502; the dotted line corresponds to the spontaneous proton transfer for singlet state. (Right) Second proton transfer from N5: the reaction coordinate is the distance between the free oxygen atom (after first proton transfer from His502) and the FAD N5 proton (from here, dotted line, the products are formed with a 27 kcal·mol^{-1} energy release). The most stable local minima are represented along the profile as "R" which stands for reactants, "Int" corresponds to the stable intermediate found after proton transfer from His502, and "P" stands for the final products.

(Figure 6, right). Local minima structures ("R", "Int", and "P" in Figure 6) along the most favorable computed reaction coordinate are depicted in Figure 7. Clearly, the large quantitative change between the triplet internal energy profiles for the C4a and proton transfer reaction coordinates (left and right in Figure 6), together with the drastic reduction of the triplet/singlet crossing point, are indicative of proton transfer mechanism. While these numbers might be slightly shifted with the inclusion of entropic corrections, the relative energy differences will remain similar. Electrostatic potential charge analyses show that, in the case of the reactants triplet state ("R"), 42% of the first electron is already found in the O_2 molecule while after proton transfer ("Int") one complete electron is already localized on the OOH group.

In addition to the wild type protein, computational studies were also performed for the two H502A and H546A variants to investigate the importance of these two histidines in O_2 reduction. In the case of H502A considerable differences relative to native AAO are observed. When freely optimized in the triplet state the O_2 molecule adopts a position above the flavin ring and part of the electron density is transferred (21%). In singlet state the O_2 molecule binds spontaneously to the C4a site where a stable intermediate is formed without proton abstraction from N5 and 69% of the electron density is found on the two oxygen atoms. The absence of the His502 also deprives the possibility for proton transfer in the initial triplet state, which has been seen to be energetically more favorable than the reaction through the C4a coordinate. In the case of the H546A variant, results are equivalent to those found for the native enzyme.
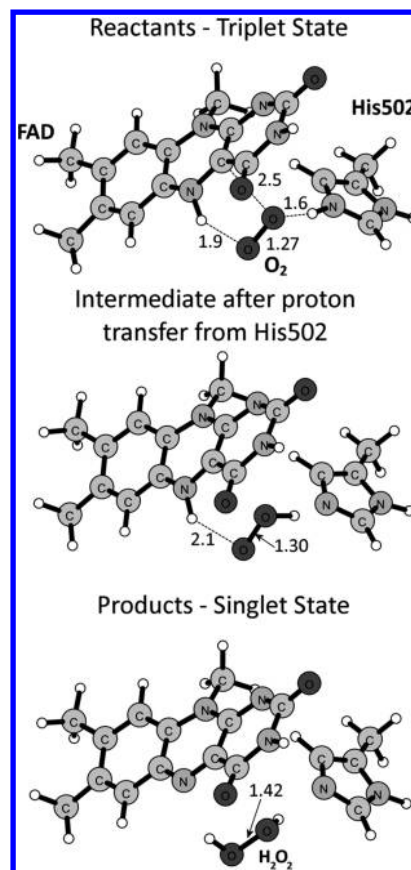

Figure 7. Local minima structures computed with QM/MM methods (the rest of the protein is not shown for simplicity purposes). Here the quantum region is displayed where the reactants − triplet state corresponds to the point "R" in the potential energy surface in Figure 6. The intermediate state, "Int", in triplet state after proton transfer from His502. Finally, the products with formation of H_2O_2 are displayed with correspondence to the "P". All distances shown are in Å (the Cartesian coordinates for the main stationary points obtained are provided in Supporting Table S3B).

■ DISCUSSION

Conserved Histidines and Substrates (Alcohol and O_2) at the AAO Active Site. The existence of an essential histidine residue in a GMC oxidoreductase was first shown by Nakanishi et al.[40] using chemical modification of glucose oxidase. After the *A. niger* glucose oxidase crystal structure was solved, it was postulated that one of its two active-site histidines (His516 and His559) would act as a catalytic base in the reductive half-reaction activating glucose, and as a catalytic acid in the oxidative half-reaction transferring the previously received proton to O_2 for H_2O_2 formation.[41] The same role for the homologous residues was suggested in AAO, after homology modeling.[5] The AAO crystal structure shows His502 and His546 in front of the *re*-side of flavin at ~4 and ~5 Å, respectively, from the N5 and C4a atoms involved in the redox reactions,[13,23] and a water molecule equidistant from N5 and His502 (but further from His546) occupying the active site cavity in the absence of substrates (Supporting Figure S7).[11] Because of its buried active site,[11] no crystal structures of AAO in the presence of substrates (or analogues) are available. Therefore, one of the first tasks for further studying the reductive and oxidative half-reactions was to diffuse substrates

from the protein surface using PELE[32] and dock them at the active-site cavity.

Diffusion of *p*-methoxybenzyl alcohol and O_2, the natural AAO substrates,[42,43] resulted in catalytically relevant positions between the flavin ring and the side-chains of His502, His546, Tyr92, and Phe501 (Figure 8). The positions predicted for the
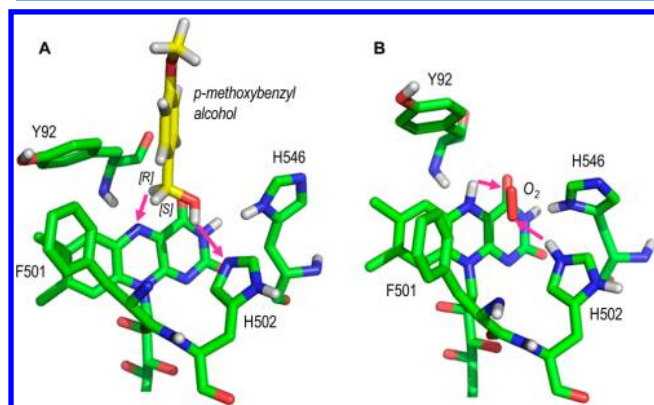
Figure 8. AAO reducing and oxidizing substrates at the active site. (A) *p*-Methoxybenzyl alcohol docking before its oxidation by the enzyme, involving hydroxyl proton and pro-R α-hydrogen abstractions (cyan arrows) by His502 and flavin N5, respectively (the latter in a hydride transfer reaction). (B) O_2 docking before its reduction to H_2O_2 by the enzyme, involving two proton transfers (together with two one-electron abstractions from the flavin). Substrate migration and docking at the active site were performed by PELE[32] based on the AAO crystal structure (PDB entry 3FIM), as previously described.[21,33]

alcohol α-carbon and the O_2 molecule are very close to that of water-586 oxygen in the crystal structure, in agreement with that suggested for glucose oxidase, where the expected O_2-binding position was occupied by water-10 in the crystal.[24] Among the above residues, Tyr92 would participate in substrate binding by aromatic stacking between the aryl-alcohol and tyrosine rings.[21] On the other hand, Phe501 would contribute to the oxidative half-reaction, as shown by the 60−80-fold lower $k_{cat}/K_{m(Ox)}$ and $k_{ox(app)}$ after mutation (Tables 1 and 2) helping O_2 to attain a catalytically relevant position near the flavin N5−C4a locus.[33] The role of the two histidine residues is discussed below.

Alcohol Oxidation Mechanism. The strong $^D(k_{cat}/K_{m(Al)})$ observed in α-dideuterated *p*-methoxybenzyl alcohol oxidation shows that abstraction of one of the substrate α-hydrogens constitutes the main limiting step in the AAO reductive half-reaction,[29] in agreement with the hydride transfer mechanism described for glucose oxidase,[44] and extended to other GMC oxidoreductases.[13] QM/MM calculations after alcohol docking at the AAO active site[30] confirmed the position of the three α-substituents shown in Figure 8A. Such a position implies a selective removal of the pro-R hydrogen by the flavin N5, as confirmed by the strong KIE observed for the (R) enantiomer of α-monodeuterated *p*-methoxybenzyl alcohol, compared with the (S) enantiomer. These findings were the first demonstration on enantioselective hydride abstraction by a GMC oxidoreductase and suggest that AAO could be of interest for deracemization of chiral secondary aryl-alcohols.[30] The consensus oxidation mechanism in GMC oxidoreductases also includes a catalytic base activating the alcohol substrate, a fact that in AAO is consistent with the requirement of an unprotonated residue, as shown by the pH profiles of the

H546S variants. However, AAO differs from other members of the superfamily (such as choline oxidase) where proton and hydride transfers are stepwise,[13] since the low $^{D_2O}(k_{cat}/K_{m(Al)})$ observed is indicative of partially limiting proton transfer concerted with the hydride transfer. A solvent KIE being indicative for a concerted reaction mechanism has also been reported for oxidation of several substrates by methanol oxidase.[45] The above is in agreement with the absence of a distinct alkoxide intermediate in the QM/MM simulations of *p*-methoxybenzyl alcohol oxidation by AAO, while similar simulations show the existence of such intermediate in the choline oxidase reaction.[21]

The two active-site histidines in AAO have a higher contribution to the rate-limiting reductive than oxidative half-reaction, as shown by the His502S/A and H546S/A variants being fully oxidized during steady-state turnover (while native AAO is ∼20% reduced). This agrees with the decreases in their transient-state constants after mutation, being much higher for enzyme reduction (1770−232000-fold lower efficiency in hydride transfer) than for enzyme reoxidation (1−12-fold lower $k_{ox(app)1}$). The identity of the catalytic base has been a matter of controversy in GMC oxidoreductases.[14−20] In AAO, removal of active-site histidines affects alcohol binding, as revealed by the increase of dissociation constants for the H502A (122-fold higher K_d) and H546A (50-fold higher K_d) variants. However, the most drastic effect is on AAO activity by the H502S/A mutations (1250−2500-fold lower k_{cat} and k_{red}), while only a moderate effect is caused by the H546S/A mutations (35−50-fold lower k_{cat} and k_{red}). Moreover, the acidic pK_a observed in the activity−pH profiles of the His546 variants was assigned to His502, since it is not observed in the profiles of the His502 variants. The above results, together with the previously reported protonation and molecular dynamics studies predicting unprotonated Nε in His502 while both Nδ and Nε in His546 would be protonated (the Nε proton shared with neighbor Glu389 carboxylate),[21] clearly point to His502 as the catalytic base in the AAO reductive half-reaction (Figure 8A) while His546 H-binds the alcohol substrate.[30]

Concerning other GMC oxidoreductases, the active-site histidine residue homologous to *P. eryngii* AAO His502 (see Figure 1) was first suggested as the catalytic base in glucose oxidase from *A. niger* (His516)[41,46] and *Penicillium amagasa-kiense* (His520), with 10000−80000-fold lower $k_{cat}/K_{m(Al)}$ after mutation[15] and more recently confirmed in *T. ochracea* pyranose 2-oxidase (His548)[20] and *P. chrysosporium* cellobiose dehydrogenase (His689).[17] Crystallographic evidence in cholesterol oxidase, where the homologous His447 was found to be ε-protonated, questioned its role as the catalytic base, and an electrostatic patch including different active-site residues has been suggested to play this role.[47] A similar hypothesis has been proposed for choline oxidase.[13,18,48] However, our QM/MM calculations suggest that His466, homologous to AAO His502, would also be the main catalytic base in choline oxidase.[21]

O_2 Reduction Mechanism. The mechanism of O_2 reduction by AAO (flavin hydroquinone form) with formation of two products (flavin quinone and H_2O_2) and one possible intermediate (C4a-hydroperoxide) was investigated using a combination of experimental and computational methods. A possible intermediate enzyme species was detected by global analysis of the spectral changes during stopped-flow reoxidation of AAO (species B in Figure 4), a similar two-step reoxidation model has been reported for cholesterol oxidase and some other flavooxidases.[49,50] However, it does not show the
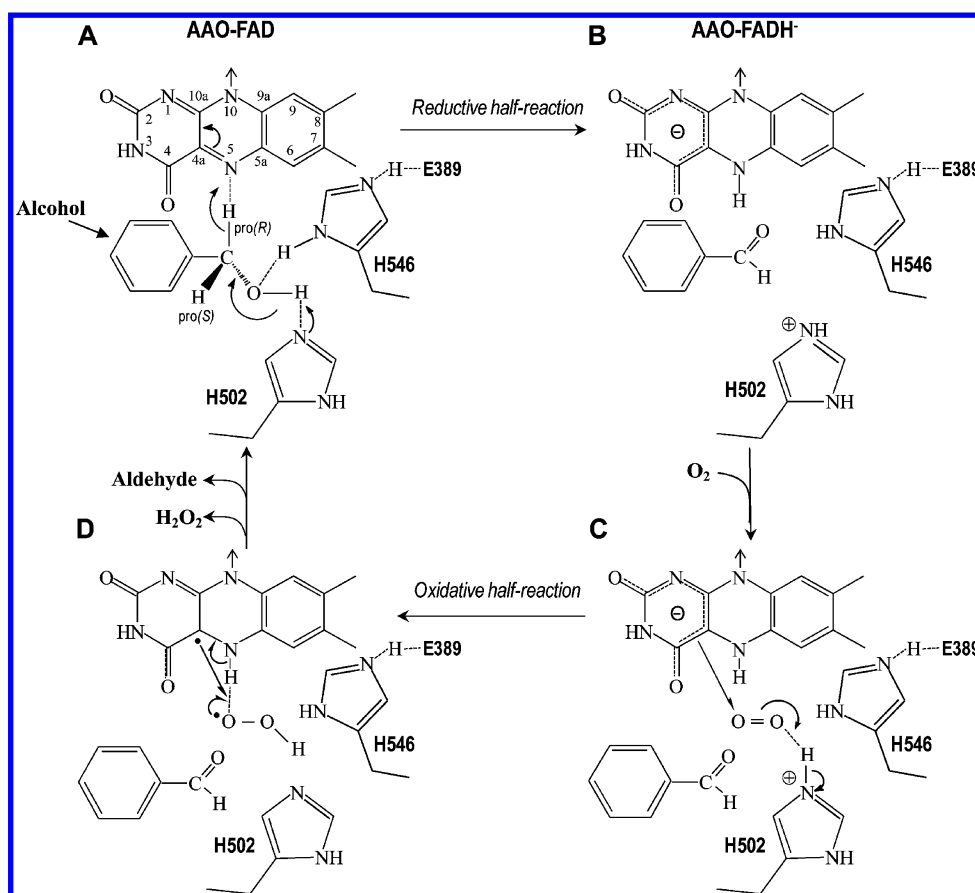
Figure 9. Scheme for the AAO catalytic cycle including reductive (top) and oxidative (bottom) half-reactions. In the first half-reaction oxidized FAD (quinone form) abstracts one hydride (two electrons plus the pro-(R) α-hydrogen) from the alcohol substrate aided by His502 as a catalytic base (abstracting the alcohol hydroxyl proton) and His546 H-bonding the alcohol at the active site (A) yielding the aldehyde product, reduced FAD (hydroquinone form) and protonated His502 (B). In the second half-reaction, the cationic His502 transfers its proton to O_2 promoting a first one-electron transfer from the ainionic flavin (C) forming a protonated superoxide radical that receives a second electron from the previously formed flavin semiquinone radical and a second proton from the flavin N5 yielding the H_2O_2 product and the two-electron oxidized FAD, without formation of a flavin hydroperoxide intermediate (D). The His546 Nε-proton is shared with neighbor Glu389.

characteristic spectrum of the flavin C4a-hydroperoxide.[51] Computational modeling supports this conclusion. Only for the small QM model we observe O_2 binding to the C4a atom, in agreement with isolated flavin oxidation studies.[52] Introducing a histidine residue (source of protons) in the QM model aiming to reproduce the active site environment (His502), drives the system spontaneously to products without formation of the hydroperoxide intermediate. The full enzyme QM/MM studies confirm the lack of covalent addition between the O_2 molecule and the flavin. Although a stable flavin-hydroperoxide intermediate has been recently found in a flavooxidase (fungal pyranose 2-oxidase),[51] and a C4a-oxygen adduct has been observed in choline oxidase upon X-ray exposure,[53] the hydroperoxide intermediate is not an obligatory species in oxidases, but it is typical for monooxygenases,[23]

The O_2 molecule docked at the AAO active site occupies approximately the same position of the alcohol substrate α-carbon, near the His502 and His546 side chains, the former being double-protonated after abstracting the hydroxyl proton in the reductive half-reaction (Figure 6B). In contrast with that observed for the reductive half-reaction, the steady-state and transient-state kinetic constants of the four histidine variants show that only His502 is significantly involved in O_2 reduction. The H502A mutation causes a 6-fold decrease of the $k_{ox(app)1}$, and up to 12-fold decrease is caused by the H502S mutation,

while the decrease caused by the H546A mutation is only 1.3-fold. Computational modeling clearly indicates that the role of His502 is (i) reducing the singlet/triplet gap to $\sim$10 kcal·mol^{-1}, as a result of a larger electron transfer from FADH$^-$ into O_2 (discussed below); and (ii) providing an initial proton into the O_2, which further reduces the energy for the spin inversion process to 3 kcal·mol^{-1}. Our computations indicates that this initial proton transfer is not a limiting step in the oxidative half-reaction (barrierless process when considering the zero point energy) in agreement with the absence of a solvent KIE on $k_{cat}/K_{m(Ox)}$ ($\sim$1), as reported also for other GMC oxidoreductases.[54,55]

It has been postulated for glucose oxidase, which became the prototype of non-metallo-oxidases for oxidative half-reaction studies,[24,55−57] that the role of the conserved active-site histidine would be to lower the barrier leading to superoxide anion and/or stabilize the superoxide formed, after the first electron transfer from the reduced flavin to O_2. In A. niger glucose oxidase, the involvement of protonated His516 in O_2 reduction is further supported by the $k_{cat}/K_{m(Ox)}$ pH profiles for the native enzyme and its H516A variant,[55] but a similar pH effect could not be demonstrated for AAO. Despite the fact that partial electron transfer on the O_2 molecule is systematically observed for the diverse QM and QM/MM calculation, the percentage of transferred electron appears to be significantly

dependent on the local environment. For the His502A mutant only 20% of the electron density is seen on the O_2. Additionally, the electron transfer using a neutral His502 (single point calculation where the ε-proton is removed from the histidine) is also reduced to 20%, confirming the importance of a charged residue for the initial electron transfer. In addition to the protonated conserved histidines, other active-site positive charges could participate in O_2 reduction by some oxidases, such as (i) the charged product of choline oxidase,[58] in agreement with the low $k_{cat}/K_{m(Ox)}$ decrease after His466 mutation;[18] or (ii) the lysine residues near the flavin N5 in monomeric sarcosine oxidase,[59] and fructosamine oxidase.[60] A role of the active site lysine in the oxidative half-reaction has also been proposed for polyamine oxidase.[61]

The proton transfer from AAO His502 drives the first full electron from the flavin to the O_2 molecule. As one could expect, this proton transfer is facilitated from the initial excess of electron giving rise to the partial superoxide. In the larger reduced QM model we find a 58% excess electron with a barrierless proton transfer. In the QM/MM model, with a lower 42% transferred electron, we find 1.5 kcal·mol^{-1} energy barrier. This initial step reduces the singlet/triplet energy gap as a result from the degeneracy breakage of the molecular oxygen antibonding orbitals (HOMO). The singlet/triplet spin crossing point, however, takes place along the second proton transfer from the N5 site, with the downhill formation of the products in the singlet state (see Figure 6). Comparing the energy barriers for the two proton transfer events, it is clear that the N5 proton is the rate limiting process, in agreement with the low but significant KIE on $k_{cat}/K_{m(Ox)}$ observed when deuterated alcohol substrates are oxidized by AAO under steady-state conditions. Under these conditions, the ^2H atom occupying the (R) position is selectively abstracted by the flavin and the isotope labeling is then transferred to its N5. The $N5^2H$ $^2H^+$-exchange rate with the solvent is slower than the enzyme reduction rate, as shown by comparing the KIE values in H_2O and ^2H_2O media and reported also for pyranose-2 oxidase.[54] Therefore, the KIE observed ($^D(k_{cat}/K_{m(Ox)})$ 1.5–1.6) indicates that N5H proton transfer to superoxide anion, or other possible intermediate oxygen species, is a partially rate-limiting step in the AAO oxidative half-reaction. Rate limiting proton transfer from flavin N5 has also been reported in H_2O_2 release from the pyranose 2-oxidase hydroperoxide intermediate.[54]

Summary on Active Site Histidines in the AAO Catalytic Cycle. According to the scheme shown in Figure 9, we conclude that His502 in front of the N5–C4a locus of AAO flavin is a key residue playing a role in both: (i) the reductive half-reaction, as the catalytic base activating the alcohol substrate for concerted hydride transfer to flavin N5 (that in AAO is stereoselectively produced from the pro-R position) in agreement with previous studies; and (ii) the oxidative half-reaction, since its charged state further activates the partial first electron transfer and provides a proton (in a nonlimiting transfer reaction accompanied by full first electron capture) which reduces the singlet/triplet energy gap and is followed by (partially rate limiting) second proton transfer from flavin concomitant with spin inversion (and second electron transfer) without formation of a hydroperoxide intermediate. His546 would play a more modest role H-bonding the alcohol substrate for correct positioning during the reductive half reaction.

ASSOCIATED CONTENT

Ⓢ Supporting Information

KIE on apparent steady-state-constants, and molecular dynamics simulation in Supporting Materials and Methods; molar absorption spectra of AAO and its His502 and His546 variants (Figure S1); pH profile for $k_{cat}/K_{m(Ox)}$ of native AAO (Figure S2); spectral changes during turnover of AAO and its His546 and His502 variants (Figure S3); spectral changes during reduction of AAO and its His546 and His502 variants by p-methoxybenzyl alcohol (Figure S4); oxidation rates of AAO and its His546 and His502 variants (Figure S5); influence of substrate concentrations on steady-state KIE values (Figure S6); partial electron density map of the AAO active site including water-586 located between the flavin N5–C4a locus and the His502 Nε (Figure S7); movie showing a QM/MM simulation of O_2 reduction by AAO with His502 contribution (flavin, O_2, His502, His546, His313, Glu389, and p-anisaldehyde in the quantum region) (Movie S1); calculated energies for O_2 reduction with different basis sets (Table S1); KIE values for apparent steady-state kinetic constants — $k_{cat(app)}$, $K_{m(Ox)(app)}$, and $k_{cat(app)}/K_{m(Ox)(app)}$ — during AAO oxidation of α-deuterated p-methoxybenzyl alcohol (R, S and dideuterated forms) at nine alcohol concentrations in H_2O buffer, and for α-dideuterated alcohol in ^2H_2O buffer (Table S2); and Cartesian coordinates for the main stationary points obtained in QM and QM/MM calculations (Table S3) in Supporting Results; and Supporting References. This material is available free of charge via the Internet at http://pubs.acs.org.

AUTHOR INFORMATION

Corresponding Author

*Phone: 34 918373112. Fax: 34 915360432. E-mail: ATMartinez@cib.csic.es (A.T.M.). Phone 34 934137727. Fax 34 934137721. E-mail victor.guallar@bsc.es (V.G.).

Author Contributions

#These authors contributed equally to this work.

Author Contributions

Aitor Hernández-Ortega, Patricia Ferreira, Milagros Medina, and Angel T. Martínez contributed to the experimental part of the work, while Fátima Lucas and Victor Guallar contributed to the computational part of the work. Although all the authors participated in the interpretation and discussion of results, Angel T. Martínez, Victor Guallar, and Milagros Medina contributed to integrate the different parts of the study.

Notes

The authors declare no competing financial interest.

■ ABBREVIATIONS USED

AAO, aryl-alcohol oxidase; $^{D,D_2O}k$, multiple deuteration KIE; ^{D_2O}k, solvent deuteration KIE; ^{D}k, substrate deuteration KIE; GMC, glucose-methanol-choline oxidase (superfamily); $k_{(app)}$, apparent kinetic constant; k_{cat}, catalytic constant; K_d, dissociation constant; KIE, kinetic isotope effect; $K_{m(Al)}$, Michaelis constant for the alcohol substrate; $K_{m(Ox)}$, Michaelis constant for the O_2 substrate; k_{obs}, observed kinetic constant; k_{ox}, reoxidation constant; k_{red}, reduction constant; MM, molecular mechanics; QM, quantum mechanics

■ REFERENCES

(1) Ferreira, P., Medina, M., Guillén, F., Martínez, M. J., van Berkel, W. J. H., and Martínez, A. T. (2005) Spectral and catalytic properties of aryl-alcohol oxidase, a fungal flavoenzyme acting on polyunsaturated alcohols. *Biochem. J. 389*, 731−738.

(2) Ruiz-Dueñas, F. J., and Martínez, A. T. (2009) Microbial degradation of lignin: How a bulky recalcitrant polymer is efficiently recycled in nature and how we can take advantage of this. *Microbial Biotechnol. 2*, 164−177.

(3) Martínez, A. T., Ruiz-Dueñas, F. J., Martínez, M. J., del Río, J. C., and Gutiérrez, A. (2009) Enzymatic delignification of plant cell wall: from nature to mill. *Curr. Opin. Biotechnol. 20*, 348−357.

(4) Varela, E., Martínez, A. T., and Martínez, M. J. (1999) Molecular cloning of aryl-alcohol oxidase from *Pleurotus eryngii*, an enzyme involved in lignin degradation. *Biochem. J. 341*, 113−117.

(5) Varela, E., Martínez, M. J., and Martínez, A. T. (2000) Aryl-alcohol oxidase protein sequence: A comparison with glucose oxidase and other FAD oxidoreductases. *Biochim. Biophys. Acta 1481*, 202−208.

(6) Hecht, H. J., Kalisz, H. M., Hendle, J., Schmid, R. D., and Schomburg, D. (1993) Crystal structure of glucose oxidase from *Aspergillus niger* refined at 2.3 Å resolution. *J. Mol. Biol. 229*, 153−172.

(7) Hallberg, B. M., Leitner, C., Haltrich, D., and Divne, C. (2004) Crystal structure of the 270 kDa homotetrameric lignin- degrading enzyme pyranose 2-oxidase. *J. Mol. Biol. 341*, 781−796.

(8) Vrielink, A., Lloyd, L. F., and Blow, D. M. (1991) Crystal structure of cholesterol oxidase from *Brevibacterium sterolicum* refined at 1.8 Å resolution. *J. Mol. Biol. 219*, 533−554.

(9) Quaye, O., Lountos, G. T., Fan, F., Orville, A. M., and Gadda, G. (2008) Role of Glu312 in binding and positioning of the substrate for the hydride transfer reaction in choline oxidase. *Biochemistry 47*, 243−256.

(10) Hallberg, B. M., Henriksson, G., Pettersson, G., and Divne, C. (2002) Crystal structure of the flavoprotein domain of the extracellular flavocytochrome cellobiose dehydrogenase. *J. Mol. Biol. 315*, 421−434.

(11) Fernández, I. S., Ruiz-Dueñas, F. J., Santillana, E., Ferreira, P., Martínez, M. J., Martínez, A. T., and Romero, A. (2009) Novel structural features in the GMC family of oxidoreductases revealed by the crystal structure of fungal aryl-alcohol oxidase. *Acta Crystallogr. D. Biol. Crystallogr. 65*, 1196−1205.

(12) Sakai, Y., and Tani, Y. (1992) Cloning and sequencing of the alcohol oxidase-encoding gene (*AOD1*) from the formaldehyde-producing asporogeneus methylotrophic yeast, *Candida boidinii* S2. *Gene 114*, 67−73.

(13) Gadda, G. (2008) Hydride transfer made easy in the reaction of alcohol oxidation catalyzed by flavin-dependent oxidases. *Biochemistry 47*, 13745−13753.

(14) Kass, I. J., and Sampson, N. S. (1998) Evaluation of the role of His447 in the reaction catalyzed by cholesterol oxidase. *Biochemistry 37*, 17990−18000.

(15) Witt, S., Wohlfahrt, G., Schomburg, D., Hecht, H. J., and Kalisz, H. M. (2000) Conserved arginine-516 of *Penicillium amagasakiense* glucose oxidase is essential for the efficient binding of β-D-glucose. *Biochem. J. 347*, 553−559.

(16) Yin, Y., Liu, P., Anderson, R. G., and Sampson, N. S. (2002) Construction of a catalytically inactive cholesterol oxidase mutant:

(17) Rotsaert, F. A. J., Renganathan, V., and Gold, M. H. (2003) Role of the flavin domain residues, His689 and Asn732, in the catalytic mechanism of cellobiose dehydrogenase from *Phanerochaete chrysosporium*. *Biochemistry 42*, 4049−4056.

(18) Ghanem, M., and Gadda, G. (2005) On the catalytic role of the conserved active site residue His466 of choline oxidase. *Biochemistry 44*, 893−904.

(19) Rungsrisuriyachai, K., and Gadda, G. (2010) Role of asparagine 510 in the relative timing of substrate bond cleavages in the reaction catalyzed by choline oxidase. *Biochemistry 49*, 2483−2490.

(20) Wongnate, T., Sucharitakul, J., and Chaiyen, P. (2011) Identification of a catalytic base for sugar oxidation in the pyranose-2 oxidation reaction. *ChemBioChem 12*, 2577−2586.

(21) Hernández-Ortega, A., Borrelli, K., Ferreira, P., Medina, M., Martínez, A. T., and Guallar, V. (2011) Substrate diffusion and oxidation in GMC oxidoreductases: An experimental and computational study on fungal aryl-alcohol oxidase. *Biochem. J. 436*, 341−350.

(22) Massey, V. (1994) Activation of molecular oxygen by flavins and flavoproteins. *J. Biol. Chem. 269*, 22459−22462.

(23) Mattevi, A. (2006) To be or not to be an oxidase: challenging the oxygen reactivity of flavoenzymes. *Trends Biochem. Sci. 31*, 276−283.

(24) Klinman, J. P. (2007) How do enzymes activate oxygen without inactivating themselves? *Acc. Chem. Res. 40*, 325−333.

(25) Gadda, G. (2012) Oxygen activation in flavoprotein oxidases: The importance of being positive. *Biochemistry*, DOI: 10.1021/bi300277d.

(26) Pennati, A., and Gadda, G. (2011) Stabilization of an Intermediate in the Oxidative Half-Reaction of Human Liver Glycolate Oxidase. *Biochemistry 50*, 1−3.

(27) Ruiz-Dueñas, F. J., Ferreira, P., Martínez, M. J., and Martínez, A. T. (2006) In vitro activation, purification, and characterization of *Escherichia coli* expressed aryl-alcohol oxidase, a unique H_2O_2-producing enzyme. *Protein Express Purif. 45*, 191−199.

(28) Macheroux, P. (1999) UV-visible spectroscopy as a tool to study flavoproteins, in *Flavoprotein Protocols* (Chapman, S., Reid, G. A., Eds.) pp 1−7, Humana Press, Totowa, USA.

(29) Ferreira, P., Hernández-Ortega, A., Herguedas, B., Martínez, A. T., and Medina, M. (2009) Aryl-alcohol oxidase involved in lignin degradation: A mechanistic study based on steady and pre-steady state kinetics and primary and solvent isotope effects with two different alcohol substrates. *J. Biol. Chem. 284*, 24840−24847.

(30) Hernández-Ortega, A., Ferreira, P., Merino, P., Medina, M., Guallar, V., and Martínez, A. T. (2012) Stereoselective hydride transfer by aryl-alcohol oxidase, a member of the GMC superfamily. *ChemBioChem 13*, 427−435.

(31) *Maestro 9.2* (2011) Schrödinger Inc., New York.

(32) Borrelli, K. W., Vitalis, A., Alcantara, R., and Guallar, V. (2005) PELE: Protein energy landscape exploration. A novel Monte Carlo based technique. *J. Chem. Theory Comput. 1*, 1304−1311.

(33) Hernández-Ortega, A., Lucas, F., Ferreira, P., Medina, M., Guallar, V., and Martínez, A. T. (2011) Modulating O_2 reactivity in a fungal flavoenzyme: Involvement of aryl-alcohol oxidase Phe-501 contiguous to catalytic histidine. *J. Biol. Chem. 286*, 41105−41114.

(34) *Jaguar 7.8* (2011) Schrödinger Inc., New York.

(35) Zhao, Y., and Truhlar, D. G. (2008) The M06 suite of density functionals for main group thermochemistry, thermochemical kinetics, noncovalent interactions, excited states, and transition elements: two new functionals and systematic testing of four M06-class functionals and 12 other functionals. *Theor. Chem. Acc. 120*, 215−241.

(36) Jensen, F. (1999) *Introduction to Computational Chemistry*, John Wiley and Sons, Chichester, UK.

(37) *QSite 4.5* (2007) Schrödinger, Inc., Portland, OR.

(38) Ferreira, P., Hernández-Ortega, A., Herguedas, B., Rencoret, J., Gutiérrez, A., Martínez, M. J., Jiménez-Barbero, J., Medina, M., and Martínez, A. T. (2010) Kinetic and chemical characterization of

aldehyde oxidation by fungal aryl-alcohol oxidase. *Biochem. J. 425*, 585−593.

(39) Abramovitz, A. S., and Massey, V. (1976) Interaction of phenols with old yellow enzyme - Physical evidence for charge-transfer complexes. *J. Biol. Chem. 251*, 5327−5336.

(40) Nakanishi, Y., Ohashi, K., and Tsuge, H. (1984) Essential histidyl residues in glucose oxidase. Chemical modification of histidyl residues with diethylpyrocarbonate. *Agric. Biol. Chem. 48*, 2951−2959.

(41) Wohlfahrt, G., Witt, S., Hendle, J., Schomburg, D., Kalisz, H. M., and Hecht, H.-J. (1999) 1.8 and 1.9 Å resolution structures of the *Penicillium amagasakiense* and *Aspergillus niger* glucose oxidase as a basis for modelling substrate complexes. *Acta Crystallogr. D. Biol. Crystallogr. 55*, 969−977.

(42) Gutiérrez, A., Caramelo, L., Prieto, A., Martínez, M. J., and Martínez, A. T. (1994) Anisaldehyde production and aryl-alcohol oxidase and dehydrogenase activities in ligninolytic fungi from the genus *Pleurotus. Appl. Environ. Microbiol. 60*, 1783−1788.

(43) Guillén, F., and Evans, C. S. (1994) Anisaldehyde and veratraldehyde acting as redox cycling agents for H_2O_2 production by *Pleurotus eryngii. Appl. Environ. Microbiol. 60*, 2811−2817.

(44) Brinkley, D. W., and Roth, J. P. (2005) Determination of a large reorganization energy barrier for hydride abstraction by glucose oxidase. *J. Am. Chem. Soc. 127*, 15720−15721.

(45) Menon, V., Hsieh, C. T., and Fitzpatrick, P. F. (1995) Substituted alcohols as mechanistic probes of alcohol oxidase. *Bioorg. Chem. 23*, 42−53.

(46) Meyer, M., Wohlfahrt, G., Knäblein, J., and Schomburg, D. (1998) Aspects of the mechanism of catalysis of glucose oxidase: A docking, molecular mechanics and quantum chemical study. *J. Comput.-Aided Mol. Des. 12*, 425−440.

(47) Lario, P. I., Sampson, N., and Vrielink, A. (2003) Sub-atomic resolution crystal structure of cholesterol oxidase: What atomic resolution crystallography reveals about enzyme mechanism and the role of the FAD cofactor in redox activity. *J. Mol. Biol. 326*, 1635−1650.

(48) Rungsrisuriyachai, K., and Gadda, G. (2008) On the role of histidine 351 in the reaction of alcohol oxidation catalyzed by choline oxidase. *Biochemistry 47*, 6762−6769.

(49) Piubelli, L., Pedotti, M., Molla, G., Feindler-Boeckh, S., Ghisla, S., Pilone, M. S., and Pollegioni, L. (2008) On the oxygen reactivity of flavoprotein oxidases - An oxygen access tunnel and gate in *Brevibacterium sterolicum* cholesterol oxidase. *J. Biol. Chem. 283*, 24738−24747.

(50) Kommoju, P. R., Bruckner, R. C., Ferreira, P., Carrell, C. J., Mathews, F. S., and Jorns, M. S. (2009) Factors that affect oxygen activation and coupling of the two redox cycles in the aromatization reaction catalyzed by NikD, an unusual amino acid oxidase. *Biochemistry 48*, 9542−9555.

(51) Sucharitakul, J., Prongjit, M., Haltrich, D., and Chaiyen, P. (2008) Detection of a C4a-hydroperoxyflavin intermediate in the reaction of a flavoprotein oxidase. *Biochemistry 47*, 8485−8490.

(52) Kemal, C., Chan, T. W., and Bruice, T. C. (1977) Reaction of $^3O_2$ with dihydroflavins. 1. N3,5-Dimethyl-1,5-dihydrolumiflavin and 1,5-dihydroisoalloxazines. *J. Am. Chem. Soc. 99*, 7272−7286.

(53) Orville, A. M., Lountos, G. T., Finnegan, S., Gadda, G., and Prabhakar, R. (2009) Crystallographic, spectroscopic, and computational analysis of a flavin C4a-oxygen adduct in choline oxidase. *Biochemistry 48*, 720−728.

(54) Sucharitakul, J., Wongnate, T., and Chaiyen, P. (2011) Hydrogen peroxide elimination from C4a-hydroperoxyflavin in a flavoprotein oxidase occurs through a single proton transfer from flavin N5 to a peroxide leaving group. *J. Biol. Chem. 286*, 16900−16909.

(55) Roth, J. P., and Klinman, J. P. (2003) Catalysis of electron transfer during activation of O_2 by the flavoprotein glucose oxidase. *Proc. Natl. Acad. Sci. U.S.A. 100*, 62−67.

(56) Su, Q., and Klinman, J. P. (1999) Nature of oxygen activation in glucose oxidase from *Aspergillus niger*: the importance of electrostatic stabilization in superoxide formation. *Biochemistry 38*, 8572−8581.

(57) Roth, J. P., Wincek, R., Nodet, G., Edmondson, D. E., McIntire, W. S., and Klinman, J. P. (2004) Oxygen isotope effects on electron transfer to O_2 probed using chemically modified flavins bound to glucose oxidase. *J. Am. Chem. Soc. 126*, 15120−15131.

(58) Finnegan, S., Agniswamy, J., Weber, I. T., and Gadda, G. (2010) Role of valine 464 in the flavin oxidation reaction catalyzed by choline oxidase. *Biochemistry 49*, 2952−2961.

(59) Zhao, G. H., Bruckner, R. C., and Jorns, M. S. (2008) Identification of the oxygen activation site in monomeric sarcosine oxidase: Role of Lys265 in catalysis. *Biochemistry 47*, 9124−9135.

(60) McDonald, C. A., Fagan, R. L., Collard, F., Monnier, V. M., and Palfey, B. A. (2011) Oxygen reactivity in flavoenzymes: Context matters. *J. Am. Chem. Soc. 133*, 16809−16811.

(61) Pozzi, M. H., and Fitzpatrick, P. F. (2010) A lysine conserved in the monoamine oxidase family is involved in oxidation of the reduced flavin in mouse polyamine oxidase. *Arch. Biochem. Biophys. 498*, 83−88.